AIAA JOURNAL
Vol. 38, No. 7, July 2000

Numerical Investigation of Instability and Transition in an Obstructed Channel Flow

Kyung-Soo Yang*
Inha University, Inchon 402-751, Republic of Korea

Instability and transition in an obstructed channel flow are investigated using direct numerical simulation. The flow geometry under consideration is a plane channel with two-dimensional thin obstacles (baffles) mounted symmetrically in the vertical direction and periodically in the streamwise direction. The flow is steady and symmetric at low Reynolds numbers. Above a certain Reynolds number, the flow undergoes a Hopf bifurcation, leading to a solution periodic in time. At high Reynolds numbers the unsteady flow exhibits a space-time symmetry-breaking bifurcation. A secondary instability is also observed at high Reynolds numbers, which is believed to be responsible for a subsequent chaotic breakdown of the flow. To study the secondary instability, we take the periodic solution, which results from the Hopf bifurcation, as the basic flow to be disturbed with small-amplitude random noise. Depending on the Reynolds number, the basic flow becomes unstable to three-dimensional disturbances, which results in a chaotic flow. The numerical results obtained are consistent with experimental findings currently available.

I. Introduction

ALTHOUGH for decades many researchers have paid much attention to hydrodynamic instability and laminar-turbulent transition, understanding of their mechanisms is far from complete. Instability and transition are dependent not only upon the Reynolds number but also on other physical factors such as the pressure gradient, freestream disturbances, wall roughness, and increasing nonlinearity among others. In addition to these, geometrical complexity has been a major obstacle to complete understanding of instability and transition, especially for the flows related to engineering application.

Recent rapid development of computer hardware and efficient numerical algorithms enabled one to perform numerical simulation to study instability and transition even in complex flows. The results obtained can serve as basic data to verify linear or weakly nonlinear theories. It is also possible for the numerical simulation to be directly compared with experiments via flow visualization. In this paper numerical simulation of instability and transition in a channel with thin baffles mounted symmetrically in the vertical direction and periodically in the streamwise direction (Fig. 1a) is presented. Flow separation occurs at the tip of the baffles, and high-shear layers are formed behind them. Instabilities at high-shear layers are often used in engineering applications such as heat exchangers, turbomachinery, or eddy generators to name a few, and a baffled channel flow is a simple model for them.

Laminar-turbulent transition is often characterized as a three-dimensional phenomenon. Excluding a bypass transition, the basic flow that results from primary instability (PI) becomes unstable to three-dimensional disturbances, and this is called secondary instability (SI). Since the 1980s, much attention has been paid to SI by many researchers. For a comprehensive review of this topic, see Herbert.[1] One of the most noticeable achievements in this field would be the SI analysis established by Herbert[1,2] based on the Floquet theory. He applied a linear stability analysis of three-dimensional disturbances to the basic flow, which is composed of a mean flow and a finite-amplitude two-dimensional Tollmien–Schlichting wave, which results from PI. However, his analysis cannot be applied to a nonlinear instability problem nor to the flows in complex geometry such as the obstructed channel under consideration.

Primary instability in two-dimensional channel flow has been well explained by a bifurcation theory.[3–5] However, research on the SI and its subsequent development in general two-dimensional channels is very rare. The geometry considered in this study is one of general two-dimensional channels. Experiments[6] showed that the flow undergoes a Hopf bifurcation above the critical Reynolds number, and above a certain Reynolds number higher than the critical one it becomes chaotic because of three-dimensional disturbances. This is different from the case of plane channel flow where the SI takes place at a subcritical Reynolds number for PI. In this study attempts are made to identify and characterize the PI and SI associated with the obstructed channel flow using a full Navier–Stokes solver. Numerical results obtained are compared with experimental findings currently available.[6] More emphasis will be placed on SI.

II. Formulation

Simulation of unsteady streamwise-periodic flow in a channel can be classified into one of the following two cases. In one case mass flux is fixed in time, but pressure difference between the inlet and outlet of the channel Δp fluctuates. In the other case mass flux fluctuates while Δp is fixed in time. For the flow geometry under consideration, as long as a finite difference scheme or its equivalent is used to discretize the full three-dimensional governing equations it is not possible to fix the mass flux exactly. Thus, the latter approach is adopted for this study.

All physical variables except Δp are nondimensionalized by mean bulk velocity of the periodic solution U_m and the channel height H. To nondimensionalize Δp, $\frac{1}{2}\rho U_m^2$ is used.

In this study continuity and incompressible unsteady Navier–Stokes equations are numerically solved:

$$\frac{\partial u_j}{\partial x_j} = 0 \tag{1}$$

$$\frac{\partial u_i}{\partial t} + u_j \frac{\partial u_i}{\partial x_j} = -\frac{\partial p}{\partial x_i} + \frac{1}{Re}\frac{\partial^2 u_i}{\partial x_j \partial x_j} \tag{2}$$

Here u_i is a velocity vector of which streamwise (x or x_1), normal (y or x_2), and spanwise (z or x_3) components are u, v, w (or u_1, u_2, u_3), respectively, and p is pressure. Re is a Reynolds number defined as $U_m H/\nu$, where ν is the kinematic viscosity.

The code uses a nonuniform Cartesian staggered grid (Fig. 1b) in a finite volume approach. The Cartesian system is most suitable for the geometry under consideration. To advance the solution in time, a fractional step method[7] is employed. The time advancement of the momentum equation is hybrid; the convective terms are explicitly advanced by a third-order Runge–Kutta scheme, and the viscous terms are implicitly treated by the Crank–Nicolson method:

Received 22 December 1997; revision received 11 June 1999; accepted for publication 18 October 1999.

*Associate Professor, Department of Mechanical Engineering, 253 Yong-Hyun-Dong, Nam-ku. Member AIAA.

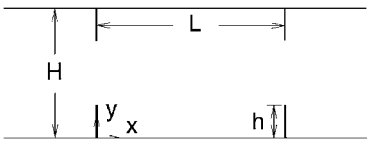

a) Geometry

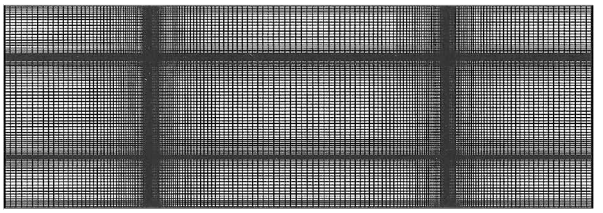

b) Typical grid

Fig. 1 Physical configuration.

$$\frac{\hat{u}_i^k - u_i^{k-1}}{\Delta t} = (\alpha_k + \beta_k)L\left(u_i^{k-1}\right) + \beta_k L\left(\hat{u}_i^k - u_i^{k-1}\right) - \gamma_k N\left(u_i^{k-1}\right) - \zeta_k N\left(u_i^{k-2}\right) - (\alpha_k + \beta_k)\frac{\partial p^{k-1}}{\partial x_i} \tag{3}$$

$$\frac{u_i^k - \hat{u}_i^k}{\Delta t} = -\frac{\partial \phi^k}{\partial x_i} \qquad (k = 1, 2, 3) \tag{4}$$

Here

$$\frac{\partial p^k}{\partial x_i} = \frac{\partial p^{k-1}}{\partial x_i} + \left(\frac{1}{\alpha_k + \beta_k} - \frac{\beta_k \Delta t}{\alpha_k + \beta_k} L\right)\frac{\partial \phi^k}{\partial x_i} \tag{5}$$

$$L = \frac{1}{Re}\frac{\partial^2}{\partial x_j \partial x_j}, \qquad N(u_i) = \frac{\partial}{\partial x_j}(u_i u_j) \tag{6}$$

where

$$\gamma_1 = \tfrac{8}{15}, \qquad \gamma_2 = \tfrac{5}{12}, \qquad \gamma_3 = \tfrac{3}{4}, \qquad \zeta_1 = 0$$

$$\zeta_2 = -\tfrac{17}{60}, \qquad \zeta_3 = -\tfrac{5}{12} \tag{7}$$

$$\alpha_1 = \beta_1 = \tfrac{4}{15}, \qquad \alpha_2 = \beta_2 = \tfrac{1}{15}, \qquad \alpha_3 = \beta_3 = \tfrac{1}{6} \tag{8}$$

$$\sum_{k=1}^{3}(\alpha_k + \beta_k) = \sum_{k=1}^{3}(\gamma_k + \zeta_k) = 1 \tag{9}$$

The spatial discretization is second-order accurate. A multigrid method is employed to solve the Poisson equation, which is obtained after the divergence-free condition is imposed on Eq. (4).

The code can compute two wavelengths of flowfield in x, which allows one to investigate a subharmonic-type instability, if any. The code is fully vectorized. It runs on a Cray Y-MP/C90 with a typical speed of 550 MFLOPS.

III. Boundary Conditions and Flow Parameters

A no-slip condition is employed at all solid boundaries including the thin baffles, and the flow is assumed to be periodic in x and z. Therefore, we actually consider an infinitely long channel with the baffles mounted periodically in x. In this study $h/H = 0.25$, $L/H = 1.456$ are chosen (Fig. 1a) to match Roberts' experiment.[6]

IV. Results and Discussion

A. Hopf Bifurcation

A fixed-pressure difference between the inlet and outlet is suddenly applied. Then the flow becomes accelerated and asymptotically approaches a symmetric solution. According to Roberts' experiments,[6] this two-dimensional symmetric solution is stable when Re is under 100. Otherwise, the flow undergoes a Hopf bifurcation leading to a solution periodic in time. This is considered as PI and remains as a two-dimensional flow.

Figure 2 shows streamlines of the steady symmetric solution at $Re = 58.5$. The flow does not undergo any instability at this Reynolds number. Roberts' experiment and his two-dimensional calculation also show the same pattern.[6] At $Re = 130$, however, the symmetric solution bifurcates to a peridic one (Fig. 3), which is identified as a Hopf bifurcation. Figure 3 shows streamlines at the same time interval for one period, and it is consistent with Fig. 6 of Roberts.[6]

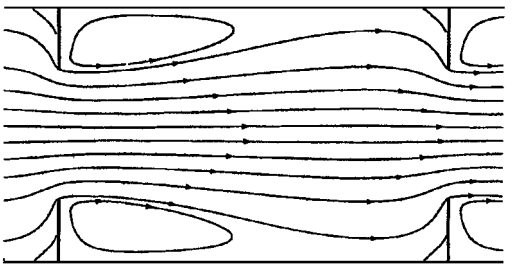

Fig. 2 Streamlines: $Re = 58.5$.

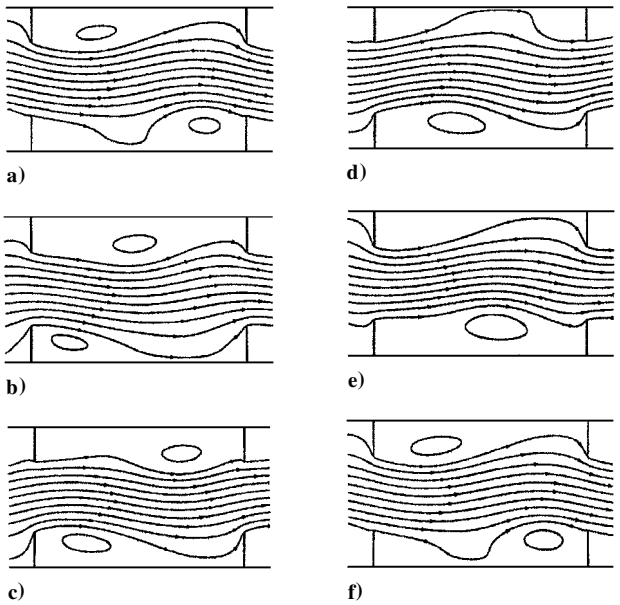

Fig. 3 Streamlines: $Re = 130$.

Figure 4 shows the time histories of the Reynolds number (Fig. 4a) and the mean magnitude of v (V_{cl}) at the centerline ($y = 0.5$, Fig. 4b). Here V_{cl} is defined as[6]

$$V_{cl} = \frac{1}{L}\int_0^L |v(x, 0.5)|\, dx \tag{10}$$

In the case of a steady solution such as in Fig. 2, the flow is symmetric in y, and obviously V_{cl} must be zero. If an instability occurs, however, the symmetry breaks up, and V_{cl} grows in time. Physically, this means that the absolute flow rate through the centerline increases. Therefore, V_{cl} can serve as a measure of the instability.[6] As a finite Δp is suddenly applied between the inlet and outlet, the Reynolds number starts growing (Fig. 4a). As the Reynolds number exceeds about 100, a Hopf bifurcation is triggered (Fig. 4b). The growth rate of the instability increases corresponding to the growth of the Reynolds number (Fig. 4b). Around $t = 30$ the Reynolds number nearly reaches its maximum and remains at that value between $t = 30$ and 40 (Fig. 4a). Thus, the growth rate is almost constant (0.4) during that time (Fig. 4b). This value is consistent with Roberts' calculation.[6] As the instability grows, the Reynolds number is decreased and finally oscillates near a mean value ($Re = 130$). The Reynolds numbers hereinafter represent the final mean values. Flow at a higher Reynolds number is obtained by accelerating the periodic flow at a lower Reynolds number. Conversely, decelerating the former yields exactly the same periodic flow as the latter. This is the case for the range of Reynolds numbers considered in this study.

The number of control volumes used to study the Hopf bifurcation is increased, depending on the Reynolds number, up to 96×96 in x and y directions, respectively. Further refinement shows less than 1% of difference in the growth rate of V_{cl}.

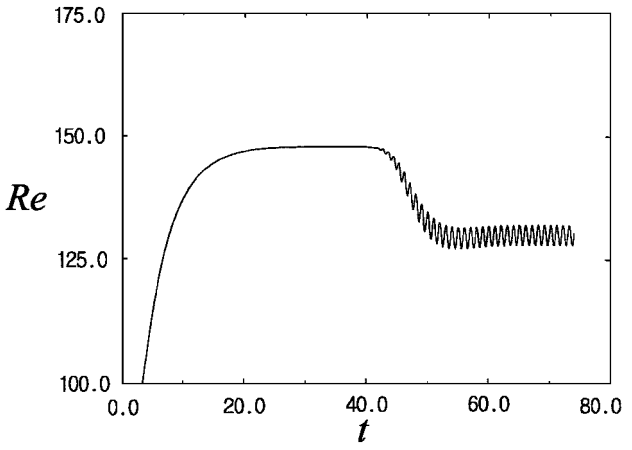

a) *Re*

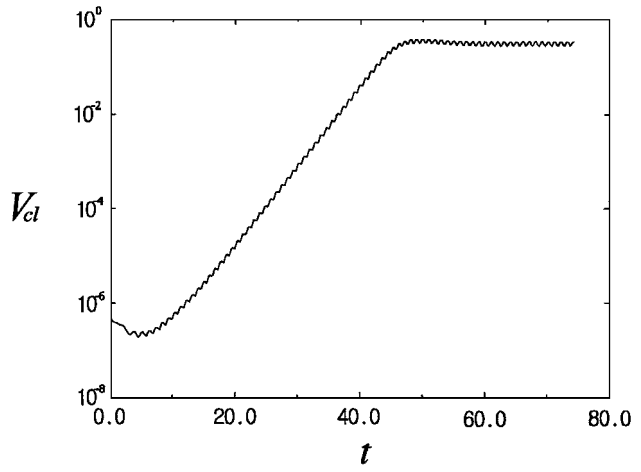

b) V_{cl}

Fig. 4 Time history.

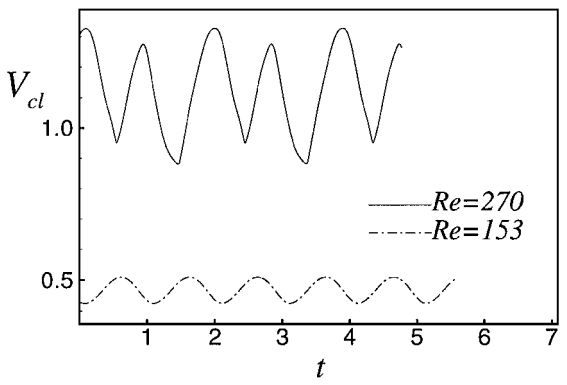

Fig. 5 V_{cl} vs time.

B. Space-Time Symmetry: Breaking Bifurcation

Figure 5 shows V_{cl} for $Re = 153$ and 270, respectively, after reaching the periodic state. In the case of $Re = 153$, the peaks correspond to the instants when the main flow between the two vertical obstacles is toward the lower or upper plane, and their magnitudes are all the same. Furthermore, the time interval between the two directions of the main flow is the same. However, these observations are not valid when the Reynolds number is high, e.g., $Re = 270$. The magnitude of V_{cl} is different for the two directions of the main flow.

For a low Reynolds number, the following space-time symmetry holds at two locations symmetric in y (Ref. 8):

$$u(x, y, t) = u(x, 1 - y, t + T/2)$$
$$v(x, y, t) = -v(x, 1 - y, t + T/2) \qquad (11)$$

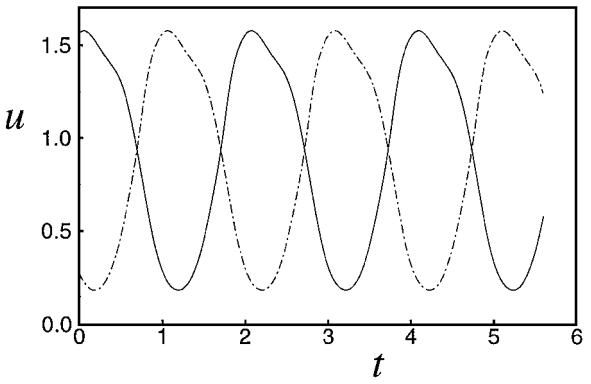

a) $Re = 153$

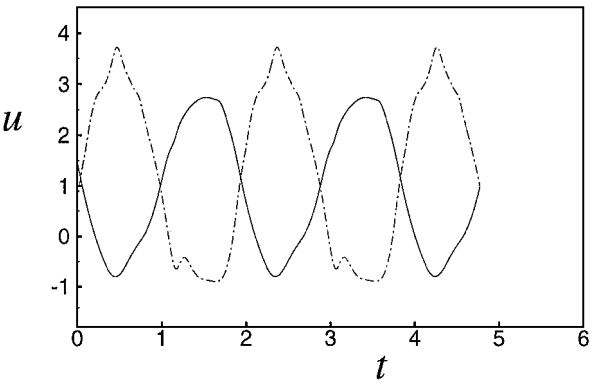

b) $Re = 270$

Fig. 6 u vs time: ——, at $x = 0.728, y = 0.25$; – –, at $x = 0.728, y = 0.75$.

where T is the period of the flow. For a high Reynolds number, Eq. (11) is no longer valid. To verify this, Figs. 6a and 6b show u at two locations symmetric in y for $Re = 153$ and 270, respectively. The period of the former is 2, and that of the latter is 1.9. The solid line represents u at $x = 0.728$, $y = 0.25$, and the broken line shows u at $x = 0.728$, $y = 0.75$. In the case of $Re = 153$, Eq. (11) holds (Fig. 6a). That is not the case for $Re = 270$ (Fig. 6b).

C. Secondary Instability

The experiment[6] also shows that the periodic flow becomes unstable to three-dimensional disturbances if the Reynolds number is approximately over 160. This is regarded to be caused by an SI associated with the flow.

For the simple flows such as a flat-plate boundary layer or a flow between two parallel plates, studies on SI have been carried out experimentally,[9,10] analytically,[1,2] and numerically,[11–14] and SI is now considered to be well understood. However, in the case of complex geometry such as ours, the basic flow is often unsteady. Research on the SI of unsteady basic flows is rare. In this investigation the full Navier–Stokes solver is used to study the characteristics of SI associated with the obstructed channel flow.

1. Criterion for Secondary Instability

To investigate SI for a given Reynolds number, a two-dimensional periodic solution is computed first. For example, Fig. 7 shows a phase plane for $Re = 183$ during $3T$ at $x = 0.728$, $y = 0.5$. The curves for each T are completely identical, which means that the flow has converged. To build an initial flowfield for a three-dimensional simulation, the two-dimensional flowfield is expanded in the spanwise direction. The resulting three-dimensional flowfield is combined with white random noise of small magnitude, at least seven orders of magnitude lower than U_m. Using this as an initial condition, a numerical solution that satisfies both continuity and Navier–Stokes equation is obtained.

The mean magnitude of $w(W_{cl})$ at an x–y plane is defined as

$$W_{cl} = \frac{1}{LH} \int_0^H \int_0^L |w(x, y, z^*)| \, dx \, dy \qquad (12)$$

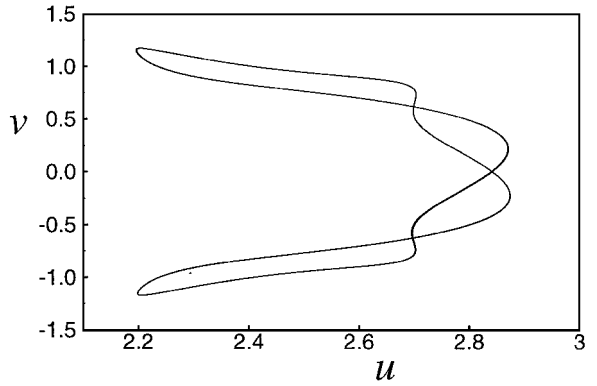

Fig. 7 Phase plane: $Re = 183$.

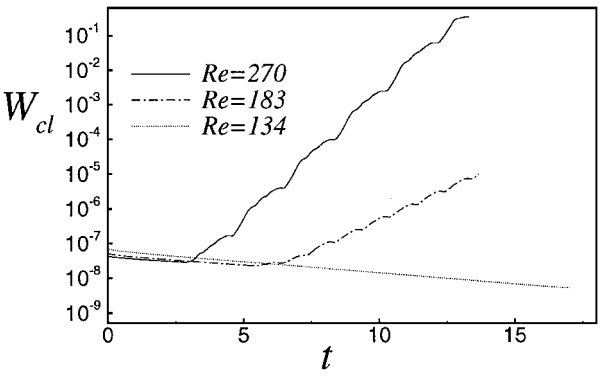

Fig. 8 W_{cl} vs time.

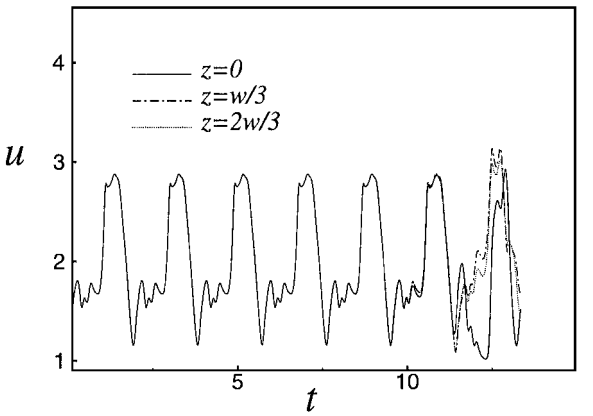

Fig. 9 Time histories of u at three spanwise locations: $Re = 270$.

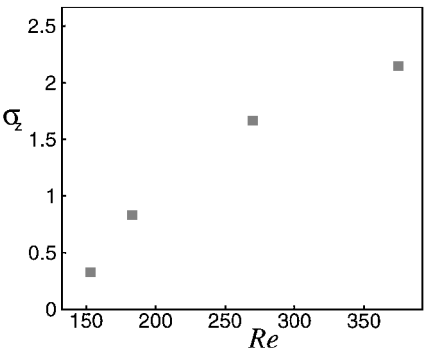

Fig. 10 Growth rate of the most unstable mode.

where z^* is an arbitrary spanwise location. If an SI occurs, W_{cl} increases, and physically this means that the absolute volume flux through the plane is increased. Therefore, the existence of an SI is detected by the behavior of W_{cl}. After a transient period in which the most unstable (the least stable) mode is established, the mode dominantly grows (most gradually decays).

This approach is similar to the previous one used to study SI in a flat-plate boundary layer.[13,14] The difference between the two approaches, however, is that in the current case the basic flow is time dependent. Therefore, normal-mode analysis cannot be applied in time.[2,15] It can still be applied in z because the flow is homogeneous in the spanwise direction.

The number of control volumes used is 96×96 in x and y directions, respectively. The resolution was proven to be adequate in the preceding two-dimensional simulation. In the spanwise direction the resolution is refined up to 96, based on the energy spectrum in z. The spanwise size of the computational domain W is chosen depending on the Reynolds number such that at least two wavelengths of the most unstable mode are contained in the domain.

2. *Linear Growth of Secondary Instability*

The behavior of W_{cl} for three different Reynolds numbers is shown in Fig. 8 in the linear-log scale. The three-dimensional computation starts at $t = 0$. For $Re = 134$ (case 1) W_{cl} monotonously decays in time, which means that the basic flow is stable to three-dimensional disturbances at this Reynolds number. For $Re = 183$ (case 2) and $Re = 270$ (case 3), however, W_{cl} grows rapidly after the initial transient period, which indicates existence of SI for these cases. Thus the critical Reynolds number for SI must be greater than 134. Furthermore, case 3 shows more rapid growth of W_{cl} than case 2, and SI also starts earlier than case 2 as expected.

Even though the basic flow is time dependent, Fig. 8 shows that the SI grows exponentially. In the cases where the SI grows (cases 2 and 3), periodicity is observed during the linear stage. This is consistent with the Floquet theory. For example, in case 3 the growth pattern of W_{cl} between $t = 6.5$ and 8.4 is identical to that between $t = 8.4$ and 10.3, and the period is the same as that of the basic flow (Fig. 6b). This could be a clue to researchers who want to carry out analytical investigations on SI of time-dependent basic flows. W_{cl} deviates from the linear growth after $t = 12.5$ because of nonlinearity. A similar trend of the behavior of W_{cl} is also noticed in case 2.

Figure 9 shows u vs t plot for case 3 at three points equispaced in z by $W/3$. All three points are taken at $x = 0.728$ and $y = 0.5$. The three curves are identical up to $t = 9.7$ because the SI is not prevailing compared with the basic flow. After $t = 9.7$, however, the SI becomes big enough to distort the basic flow, and the three curves deviate both in magnitude and in phase.

The growth rate of the most unstable mode (σ_z) can be obtained during the exponential growth of W_{cl}. Figure 10 shows σ_z at various Reynolds numbers. As the Reynolds number decreases, so does σ_z. From Fig. 10 the critical Reynolds number for SI is estimated to be between 134 and 150, which is close to the experimental observation.[6]

3. *Dominant Three-Dimensional Modes*

To identify the dominant three-dimensional modes, the spanwise profiles of w at $x = 0.728$ and $y = 0.5$ at three different times ($t = 7.0$, 9.7, 13.8) are shown in Fig. 11 for case 3. The spanwise wave numbers k_z of the dominant three-dimensional modes are obtained by Fourier transforming the profiles in Fig. 11. Figure 12 reveals the energy $|\hat{w}|^2$, where $|\hat{w}|$ is the Fourier coefficient, of each mode at $t = 9.7$ and 13.8. For clarity the modes of which energy is below 10^{-3} are not shown. In the linear stage ($t = 9.7$), $k_z = 12.56$, and its harmonic is dominant. The same wave-number selection was observed at $t = 7.0$. For a bigger $W(= 4H)$ the wave-number selection turns out to be the same. The mode of $k_z = 6.28$ also has considerable energy. This is consistent with a previous investigation of natural transition,[14] which says that multiple waves become dominant in the linear stage of natural transition. In the nonlinear stage (Figs. 11c and 12) there is significant change in energy distribution among various modes caused by nonlinear interaction between three-dimensional modes. Simulation must stop at this point because of lack of resolution. Figure 13 shows k_z of the most unstable mode. As the Reynolds number decreases, so does k_z, and it appears to go to zero at the critical Reynolds number.

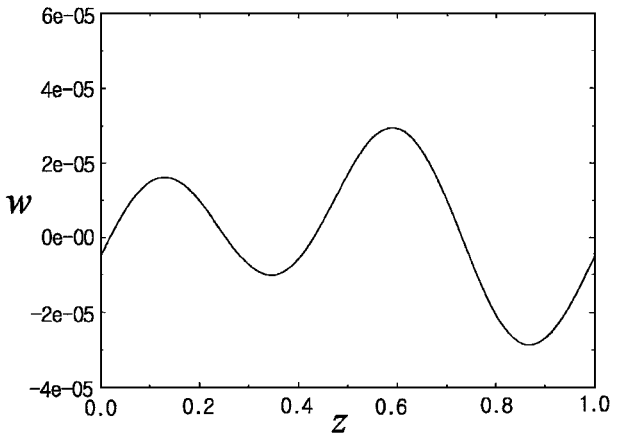

a) $t = 7.0$

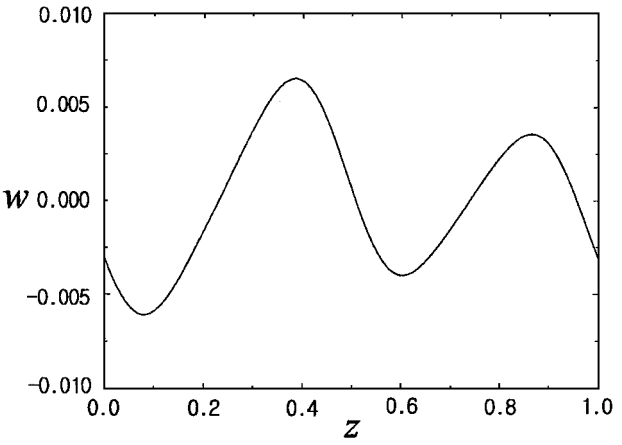

b) $t = 9.7$

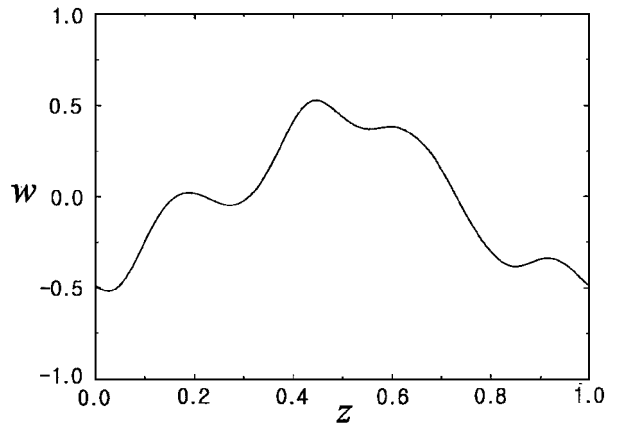

c) $t = 13.8$

Fig. 11 Profiles of w in z: $Re = 270$.

The shape of the most unstable mode for case 3 at $t = 9.7$ is shown in Fig. 14, where w contours are taken at a typical x–y plane. Solid lines represent positive values, and dotted lines negative ones with $\Delta w = 0.00078$. Contours $W/2$ apart in z are almost identical. Thus one can estimate that two wavelengths are contained in the computational domain. This is consistent with Fig. 11 and Roberts's experiment (Fig. 15 of Roberts[6]).

4. Flow Visualization

For a qualitative comparison with experimental flow visualization (Fig. 15 of Roberts[6]), Fig. 15 shows streamlines of $Re = 270$ at a nonlinear stage in a perspective view. The starting points of the streamlines are located at $x = 0.728$, $y = 0.6$, and equispaced in z. The horizontal lines in the spanwise direction represent the baffles. The flowfield is clearly three dimensional, and one can notice that the flow is more distorted near the baffles. Figure 16 is a velocity

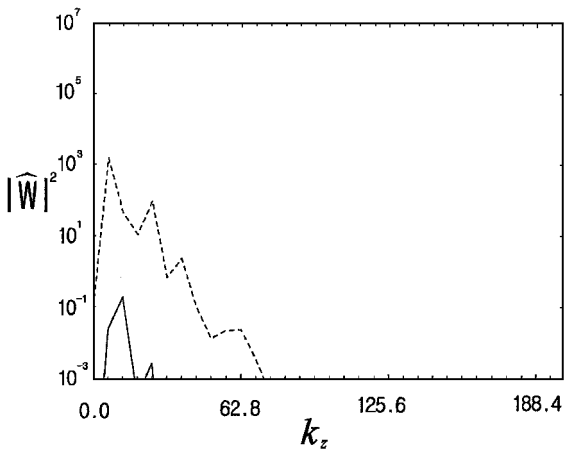

Fig. 12 Energy of spanwise Fourier modes; $Re = 270$: ——, $t = 9.7$; - - - -, $t = 13.8$.

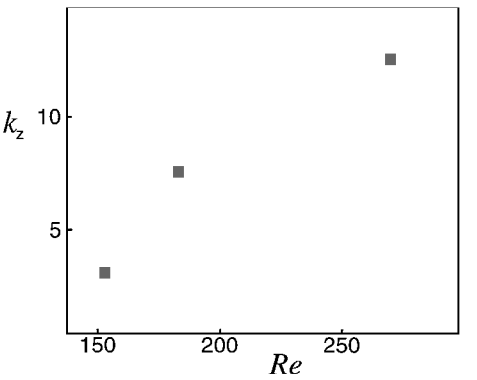

Fig. 13 Spanwise wave number of the most unstable mode.

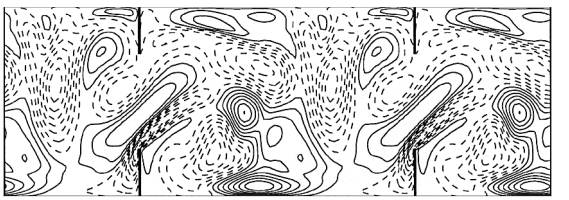

Fig. 14 Most unstable mode of w at a typical x–y plane: $Re = 270$, $t = 9.7$.

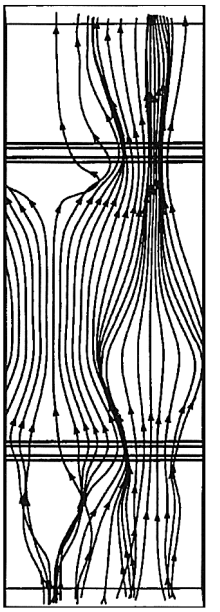

Fig. 15 Streamlines: $Re = 270$.

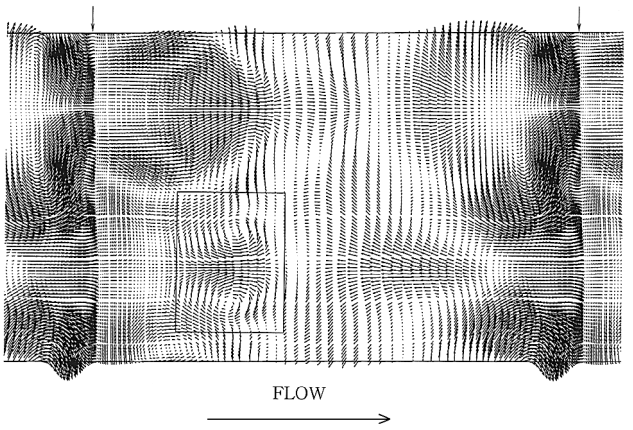

Fig. 16 Velocity vector plot: $Re = 270$, $y = 0.25$.

vector plot of $Re = 270$ at $y = 0.25$ at the same time as Fig. 15. For clarity only u and w are used to plot. The vertical arrows indicate the locations of the baffles. In the place indicated by a box, a pair of counter-rotating vortices can be noticed. All of these visual observations are consistent with those of Robert's experiments.[6]

V. Conclusions

In this investigation instability and transition in an obstructed channel flow are studied using direct numerical simulation. The flow geometry under consideration is a plane channel with two-dimensional thin obstacles mounted symmetrically in the vertical direction and periodically in the streamwise direction.

A fixed-pressure difference is suddenly imposed between inlet and outlet. Then the flow accelerates and asymptotically approaches a steady symmetric solution. Above a certain Reynolds number the flow subsequently undergoes a Hopf bifurcation leading to a solution periodic in time. At further higher Reynolds numbers a space-time symmetry-breaking bifurcation is observed.

Above a threshold value of the Reynolds number, the periodic flow becomes unstable to three-dimensional disturbances, resulting in full transition. This secondary instability, for which the critical Reynolds number is estimated to be between 134 and 150, exhibits an exponential growth in the linear stage although the basic flow is time dependent. The corresponding energy spectrum reveals that the most dominant spanwise wave number is small near the critical Reynolds number. The numerical result is qualitatively and quantitatively consistent with the experimental result currently available. The result obtained can serve as a database for verifying an analytical study associated with the flow.

Acknowledgments

The author is grateful to E. P. L. Roberts for useful discussion during this study. The author wishes to acknowledge the financial support of the Korea Research Foundation made in the program year 1996. Computations in the present work were carried out by using the Cray C90 of the Korea Research and Development Information Center supercomputing center in Korea, which is gratefully acknowledged.

References

[1]Herbert, Th., "Secondary Instability of Boundary Layers," *Annual Review of Fluid Mechanics*, Vol. 20, 1988, pp. 487–526.

[2]Herbert, Th., "Subharmonic Three-Dimensional Disturbances in Unstable Plane Shear Flows," AIAA Paper 83-1759, Jan. 1983.

[3]Sobey, I. J., and Drazin, P. G., "Bifurcations of Two-Dimensional Channel Flows," *Journal of Fluid Mechanics*, Vol. 171, 1986, pp. 263–287.

[4]Fortin, A., Fortin, M., and Gervais, J. J., "A Numerical Simulation of the Transition to Turbulence in a Two-Dimensional Flow," *Journal of Computational Physics*, Vol. 70, 1987, pp. 295–310.

[5]Fearn, R. M., Mullin, T., and Cliffe, K. A., "Nonlinear Flow Phenomena in a Symmetric Sudden Expansion," *Journal of Fluid Mechanics*, Vol. 211, 1990, pp. 595–608.

[6]Roberts, E. P. L., "A Numerical and Experimental Study of Transition Processes in an Obstructed Channel Flow," *Journal of Fluid Mechanics*, Vol. 260, 1994, pp. 185–209.

[7]Kim, J., and Moin, P., "Application of a Fractional Step Method to Incompressible Navier–Stokes Equations," *Journal of Computational Physics*, Vol. 59, 1985, pp. 308–323.

[8]Roberts, E. P. L., and Mackley, M. R., "The Development of Asymmetry and Period Doubling for Oscillatory Flow in Baffled Channels," *Journal of Fluid Mechanics*, Vol. 328, 1996, pp. 19–48.

[9]Saric, W. S., Kozlov, V. V., and Levchenko, V. Y., "Forced and Unforced Subharmonic Resonance in Boundary-Layer Transition," AIAA Paper 84-0007, Jan. 1984.

[10]Williams, D. R., Fasel, H., and Hama, F. R., "Experimental Determination of the Three-Dimensional Vorticity Field in the Boundary-Layer Transition Process," *Journal of Fluid Mechanics*, Vol. 149, 1984, pp. 179–203.

[11]Orszag, S. A., and Kells, L. C., "The Transition to Turbulence in Plane Poiseuille Flow and Plane Couette Flow," *Journal of Fluid Mechanics*, Vol. 96, 1980, pp. 159–206.

[12]Orszag, S. A., and Patera, A. T., "Secondary Instability of Wall-Bounded Shear Flows," *Journal of Fluid Mechanics*, Vol. 128, 1983, pp. 347–385.

[13]Spalart, P. R., and Yang, K.-S., "Numerical Study of Ribbon-Induced Transition in Blasius Flow," *Journal of Fluid Mechanics*, Vol. 178, 1987, pp. 345–365.

[14]Yang, K.-S., Spalart, P. R., and Ferziger, J. H., "Numerical Studies of Natural Transition in a Decelerating Boundary Layer," *Journal of Fluid Mechanics*, Vol. 240, 1992, pp. 433–468.

[15]Drazin, P. G., and Reid, W. H., *Hydrodynamic Stability*, Cambridge Univ. Press, Cambridge, England, U.K., 1981, pp. 353, 354.

D. S. McRae
Associate Editor